



Effect of Velocity on Erosion Performance of 13Cr₄Ni and H.V.O.F. Coatings

Mithlesh Sharma, D.K. Goyal* ,Naresh Kumar** and Raman Sharma**

Department of Mechanical Engineering, IET Bhaddal, (P.B.)

*Department of Mechanical Engineering, B.B.S.B.E.C. Fatehgarh, (PB)

**Department of Mechanical Engineering, SIET, Bilaspur, (H.P.)

(Received 15 March, 2012 Accepted 10 April, 2012)

ABSTRACT : The slurry erosion of two coatings applied by high velocity oxy fuel (H.V.O.F.) processes onto shot-blasted 13Cr₄Ni steel was studied, and the results were compared to those obtained with 13Cr₄Ni, which are commonly used for hydraulic turbines and accessories., while the microstructure and worn surfaces were characterized by optical and scanning electron microscopy. Slurry erosion tests were carried out in a modified impact test rig, in which the samples were placed conveniently to ensure grazing incidence of the particles. the slurry was compose of distilled water and quartz sand particles with an average diameter between 165 μm (AFS 50/70) and the slurry concentration content was 20000 ppm in all the tests. the three different ranges of velocity is taken i.e. 25m/s, 60m/s and 80m/s. at normal impact angle and comparison regarding the erosion resistance was determined from the mass loss results. Higher erosion will be seen at medium range of velocity i.e. at 60m/s. the coated surfaces showed higher erosion resistance than the uncoated stainless steels, with the lower volume losses measured for the Cr₂O₃ deposit. SEM analysis of the worn surfaces revealed intense plastic deformation in both coated and bare stainless steels, with little evidence of brittle fracture in the microstructure. The measured adhesive strength of the coatings was considered acceptable for the processes employed.

Keyword : HVOF coatings, slurry erosion, microstructure, thermal coating.

I. INTRODUCTION

Stainless steels are widely used in hydroelectric power plants due to their good corrosion properties and acceptable resistance to solid particle erosion, since many components are in contact with aqueous solutions containing hard particles that impact against the surface causing significant material loss (slurry erosion condition). The magnitude of the damage caused is a consequence of the amount, type and size of solid particles in the flow, together with the mechanical properties of the surfaces, physical-chemical properties of the water and operating conditions [1, 2]. Slurry erosion problems are particularly important during rainy seasons due to the increase in the number of solid particles impacting the surfaces, especially in systems where an exhaustive filtration process is not possible. This is the case of the Francis turbines installed in a hydroelectric power plant in north western Colombia, where intense erosive wear has led to changes in surface texture and loss of adjustment between the liners and the spiral case, as can be seen in Fig. 1. The angle of incidence of the particles is extremely important to determine the main wear mechanism acting on the surface of the components submitted to erosion. It is well known that micro-cutting prevails for low impact angles whereas for angles close to 90° the dominant effects are low-cycle fatigue and accumulation of plastic deformation up to a critical value that promotes material detaching [3, 4]. In addition, corrosive attack and boundary layer effects develop when the particles are carried by a liquid, configuring a much more intricate situation that is affected

by the rheological properties of the carrying fluid such as its density and viscosity [5, 6]. A cost-effective way to improve the slurry erosion resistance of the components is the application of thermally sprayed coatings [7, 8]. The term thermal spray describes a family of processes that use chemical or electrical energy to melt (or soften) and accelerate particles of a material which is then deposited on a surface [9]. The coatings may have a good erosion resistance depending on the chemical and mechanical properties of the material deposited, the surface preparation prior to application and the deposition conditions [7-9]. The high-velocity oxy-fuel (HVOF) process belongs to the family of thermal spraying techniques, and is widely used in many industries to protect the components against erosion, corrosion and wear. Particle degradation and open porosity are the two important factors that affect corrosion and erosion resistance. HVOF processing did not degrade significantly the composition of the consumable and has been shown to produce coatings with low porosity, low oxide content, better density, better coating cohesive strength and bond strength than many thermal spray processes [10, 11].

In this work, two thermally sprayed coatings were studied in laboratory in order to evaluate their potential application in a particular component of a Francis hydraulic turbine. The evaluation included the analysis of the worn component and comparison between coated and uncoated samples submitted to controlled slurry erosion conditions.

II. MATERIAL AND METHODS

A. Selection of Substrate Material

Steel 13 Cr₄Ni steel which is used as material for Hydro power plants in some plants in northern part of India has been used as a substrate in the study. The specimens with approximate dimensions of 40 mm × 40 mm × 5 mm were cut from the turbine material for erosion studies. Samples were grinded with SiC papers down to 180 grit and Shot -blasted with SiO₂ before being HVOF sprayed to develop better adhesion between the substrate and the coating. stainless steels commonly used for turbines and hydraulic accessories were used, namely 16 Cr₅Ni steel, whose nominal chemical compositions are shown in Table 1 Also, two commercial powders, Cr₂O₃ and CrC + NiCr were deposited onto 13 Cr₄Ni steel by High Velocity oxy fuel (HVOF) processes, respectively spraying was carried out using a HIPOJET 2100 equipment (M/S Metallizing Equipment

Co. Pvt. Ltd., Jodhpur, India), which utilize the supersonic jet generated by the combustion of liquid petroleum gas (LPG) and oxygen mixture. LPG fuel gas is cheap and readily available as compared to other fuels used for HVOF spraying. The spraying parameters employed during HVOF deposition are listed in Table 1. All the process parameters, including the spray distance were kept constant throughout the coating process.

Table 1: Nominal chemical composition of the substrate materials (wt %).

Materials	C	Mn	Si	Cr	Ni	P	S
13Cr ₄ Ni	0.06	0.80	0.261	13	15-17	0.70-1.50	4-6
Cr ₂ O ₃				90			
CrC-NiCr	30.81	18.36		50.84			

B. Apparatus Required

Measurement of Coating Thickness

1. The coating thickness was measured during spraying with a Minitest-2000 Thin Film

Thickness Gauge (precision ± 1 μm), to obtain coating of uniform thickness. For verification of thickness of deposited coating, the as sprayed specimen was cut across the cross-section with a diamond cutter.

2. X-Ray Diffraction (XRD) Analysis the XRD analysis was performed on the coated and uncoated specimens to

identify the various phases present on their surfaces.

Table 3 : Spray parameters employed for HVOF spray process.

Oxygen flow rate	250 l/min
Fuel (LPG) flow rate	60 l/min
Air-flow rate	700 l/min
Spray distance	200 mm
Powder feed rate	26 g/min
Fuel pressure	588 kPa
Oxygen pressure	883 kPa
Air pressure	588 K

The microstructure characterization was done in a JEOL 5910LV SEM at IIT, ROPAR. The porosity of the coatings was measured by digital image analysis. Vickers hardness and micro-hardness measurements were performed by using a Wolpert hardness tester (HV62.5 kg f) and a Shimadzu micro-hardness tester (HV300 g, 15 s), respectively. Localized chemical analyses of the specimens were done with an EDS spectrometer coupled to the SEM. The 13Cr₄Ni stainless steel samples were manufactured from the mithla castings. The material taken from the larji power station presented accelerated wear damage which we can easily see with the help of Fig. 1.

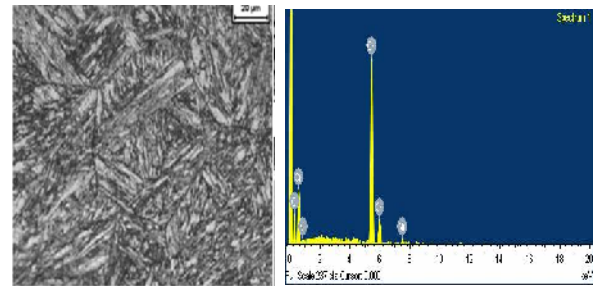


Fig. 3. Microstructure of 13CR4NI stainless steel, 500×, SEM The arrow shows a chromium carbide precipitated at the grain boundary of prior austenite.

C. Slurry erosion tests

The slurry erosion testing is conducted out in a modified test rig which is known as JET IMPACT TEST RIG in which the specimens were subjected to the erosion conditions which are very much similar to those of the hydro power plant

Fig. 2 shows the configuration of the testing machine, which is composed of a commercial centrifugal pump connected to an electrical motor, a flow discharging apparatus, flow meter and an isothermal bath to control the slurry temperature. The flow meter is used to vary the flow rate as we have to study the erosion conditions at different velocity ranges. The samples were located at the outlet of

the nozzle which is carrying out the water coming out from the outlet of centrifugal pump to ensure grazing incidence of the particles (Fig. 2). The slurry was composed of distilled water and quartz particles with a particle size distribution which will lead to average diameter of 155 micronmeter and the solids content was 30000 ppm. The mean impact velocity of the slurry was 35 m/s, 55m/s and 70m/s and the erosion resistance was determined from the mass loss results. Mass losses were measured every 30 min by using measuring balance which is having a accuracy a scale with 0.01 mg resolution. The total duration of each test was 120 min, and after that period both the sample and the slurry were replaced.

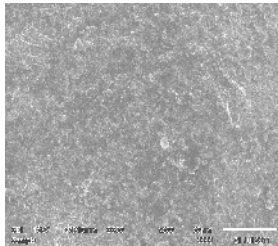


Fig. 4. Microstructure of ASTM 13Cr₄Ni steel, after coating Cr₂O₃.

Analysis of worn surfaces

The worn surface were analyzed in stereoscopic and scanning electron microscopes in order to identify the wear mechanism and relate them to the mass loss results

III. RESULTS AND DISCUSSION

A. Microstructure

(i) 13 Cr4Ni steel

The microstructure of this steel is composed of austenitic-martensitic steel with delta ferrite and about 20 to 25 stable austenite. Chromium carbides precipitated at the prior austenite grain boundaries, as can be seen in Fig. 3. The average hardness measured was 20 HV62.5 kg f. Micro-hardness measurements reported 332 HV25 g f, 15 s. in the martensitic matrix.

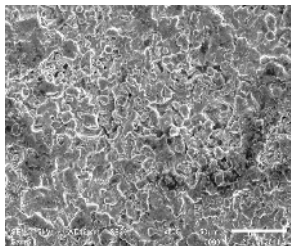


Fig. 5. Microstructure of 13Cr4Ni steel after coating with with CrC-NiCr.

(ii) Cr₂O₃ Coating

Fig. 5 shows the microstructure of a typical coating with a thickness of coating 200µm. The coating layer is

composed by a soft, nickel-rich matrix (191 HV average hardness) containing elongated chromium oxide particles (1120 HV25 g f, 15 s). The measured average volume fractions of Cr₂O₃ particles and pores were 15% and 9%, respectively. The wear-resistant Cr₂O₃ coating is composed of hard, Cr particles (1120 HV average hardness) and softer Ni-Cr regions (639 HV average hardness), together with a number of unmelted particles and pores. The volume fraction of pores was estimated to 15% by digital image processing of SEM images. This porosity amount is acceptable for HVOF coatings [10]. This average value is in agreement with literature for the HVOF process [9, 10] and it is an indication of acceptable quality of the coating.

(iii) CrC-NiCr coating

The microstructure of CrC-NiCr coating can be seen in Fig. 5. The thickness of the coating was circa average 150-200 µm. The microstructure of the wear-resistant coating CrC-NiCr (690 HV300 g, 15 s) is a distribution of chromium carbides in a high carbon steel matrix. The measured volume fraction of chromium carbides and porosity were 12% and 15%, respectively.

B. Examination of worn surfaces

The typical aspect of the worn surfaces as seen in stereographic microscope is shown in Fig. 6. Detailed analysis of the worn surfaces revealed wear marks typical of erosion at grazing incidence, with micro-cutting and micro-ploughing as the main wear mechanisms observed at the surface of all the stainless steels tested and the Cr₂O₃ coating (Fig. 7), being these marks more evident and evenly distributed in the stainless steel samples. The SEM image on micrographs tells us about the surface morphology of the various samples. The 13Cr4Ni steel has shown platelet mechanism which is being operationalized in erosion. The formation of crater and lips can be viewed. These are formed due direct impact and can be removed by impact of slurry. Fig shows splat by splat lamellar structure formation in both the coatings with the presence of partially melted region of the nano particles in Cr₂O₃ coatings. On the other hand, the worn surfaces of the CrC-NiCr coatings showed a differential response as a function of the phases present in the microstructure, as shown in Fig. 9. Chromium and oxides in Cr₂O₃ and Cr/Co areas in CrC-NiCr coatings contributed to increase the wear resistance due to their high hardness and Young modulus. As the testing time increased the hard phases were gradually exposed to the erosive particles and the main wear mechanism changed from micro cutting of matrix to spalling of hard phases. Evidences of brittle fracture were observed in the CrC-NiCr coating, as can be seen in Fig. 9 (arrow in left upper corner). Nevertheless, the analysis of the coatings before the slurry erosion tests reveals that similar cracks are formed as a consequence of the thermal spray process employed, due to the high cooling speeds and the thermal coefficient mismatch between CrC/Co

particles and Ni-Cr regions (Fig. 10). Unmelted particles and droplets can also be observed before the surface is submitted to the slurry wear tests, but these features are removed during the tests due to their low adherence to the substrate. A significant increase in micro-hardness was observed in the stainless steels surfaces after the slurry erosion tests, probably as a consequence of both martensitic transformation of retained austenite and work hardening effect.

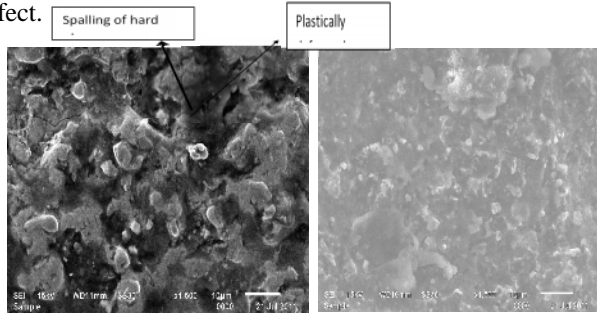


Fig. 6. specimen after conducting 2hrs erosion testing coated with CrC-NiCr Fig. 7 specimen after conducting 2Hr erosion testing coated with Cr₂O₃.

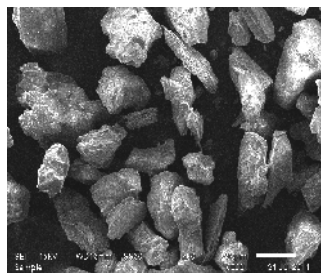


Fig. 7(a) Morphology of the sand particle used in the tests

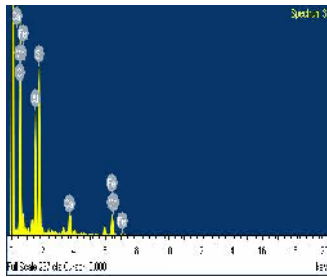


Fig. 7(b) EDS of sand grains

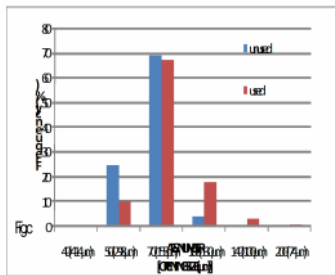


Fig. 7(c) grain size distribution before and after the test in micrometers.

C. Degradation of abrasive particles

The typical morphology of abrasive particles before the tests and the change in size distribution as a consequence of the erosive process are presented in Fig. 7. Note that after the tests the distribution is shifted to smaller grain sizes, which reveals fragmentation of the particles and subsequent loss of their ability to erode the surface of the samples.

D. Mass loss

The mass loss of all the samples in the slurry erosion tests is shown in Fig. 8. The reported values were calculated from the measured cumulative mass losses and time of impacting of particles of each of the materials studied, namely 1. Generally speaking, in all the cases the uncoated steels reported higher volume losses than the thermal sprayed coatings. The Cr₂O₃ coating showed the best erosion resistance in all the velocity ranges, while the CrC-NiCr steel reported the higher mass losses of the tested materials with coating. It is worth noticing that the uncoated stainless steels presented similar volume losses during the first stages of the tests (Fig. 8). Nevertheless, after 90 min testing the 13Cr₄Ni steel samples undoubtedly showed better erosion resistance, probably due to the differences in microstructure such as the presence of hard chromium carbides precipitated at grain boundaries. The one another important thing to be noted down that as the velocity ranges increases the amount of erosion also increase up to the 55 m/s after going higher range of velocity the erosion is not linear with respect to other two velocities. This may be due to that as the velocities is increasing the kinetic energy of the particle also increases as a result of which the particles are rebounded back and they interrupt the path of incoming particles. The maximum erosion will takes place at 55 m/s.

IV. CONCLUSIONS

- (i) The Cr₂O₃ coating applied by HVOF process onto 13Cr4Ni stainless steel reported the best slurry erosion resistance of the studied materials, in all the cases mainly as a consequence of the combined properties of hard, wear-resistant particles and a ductile metallic matrix.
- (ii) The study shows the performance of the steel and coating with arrange of velocity.
- (iii) The effect of increasing the velocity is also studied with the help of this study.
- (iv) The studied coatings showed ability to deform plastically when submitted to slurry erosion conditions, with little evidence of mass removal by brittle fracture mechanisms. Unmelted particles and droplets are easily removed from the surface, but this does not affect the overall performance of the coatings in terms of volume loss and main wear mechanisms.

(v) The applied coatings are an interesting alternative to enhance the wear resistance of components used in hydraulic machines, in particular under grazing incidence conditions and moderate-to-low mean impact velocities.

REFERENCES

- [1] J. Hengyun, *et al.*, The role of sand particles on the rapid destruction of the cavitation zone of hydraulic turbines, *Wear* **112**, 199-205(1986).
- [2] T.H. Kosel, Solid particle erosion, in: *ASM Handbook*, vol. 18, Friction, Lubrication and Wear Technology, ASM International, pp. 199-210(1992).
- [3] I.M. Hutchings, *Tribology: Friction and Wear of Engineering Materials*, Edward Arnold, Cambridge, (1992).
- [4] K.H. Zum Gahr, *Microstructure and Wear of Materials*, Elsevier, Amsterdam, (1987).
- [5] G. Sundararajan, *A comprehensive model for the solid particle erosion of ductile Materials*, *Wear* **149**, 111-127(1995).
- [6] A.V. Levy, P. Yau, Erosion of steels in liquid slurries, *Wear* **98**, 163-182(1984).
- [7] K. Sugiyama, *et al.*, Slurry wear and cavitation erosion of thermal-sprayed cermets, *Wear* **258**, 768-775(2005).
- [8] P. Kulu, I. Hussainova, R. Veinthal, *Solid particle erosion of thermal sprayed coatings*, *Wear* **258**, 488-496(2005).
- [9] D. Crawler, Thermal spray processes, in: *Handbook of Thermal Spray Technologies*, ASM International, (2004).
- [10] B.K. Prasad, Slurry wear characteristics of zinc based alloy effect of sand content of slurry silicon.

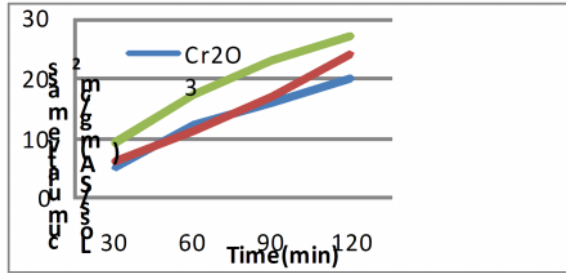


Fig. 8. cumulative mass loss after slurry erosion tests at 40m/s.

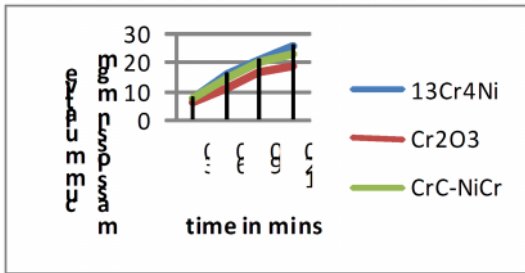


Fig. 9. cumulative mass loss after slurry erosion tests at 80m/s.

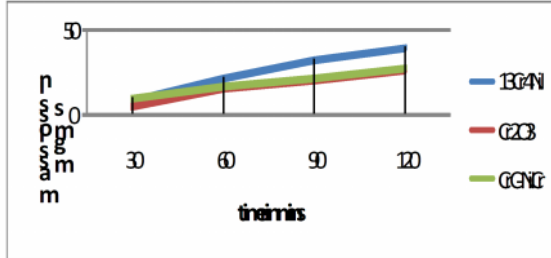


Fig. 10. cumulative mass loss after slurry erosion tests at 60m/s.